

ShareCMP: Polarization-Aware RGB-P Semantic Segmentation

Zhuoyan Liu Bo Wang* Lizhi Wang Chenyu Mao Ye Li
Harbin Engineering University

{liuzhuoyan,wb,wanglizhi111,maochenyu,liye}@hrbeu.edu.cn

Abstract

Multimodal semantic segmentation is developing rapidly, but the modality of RGB-Polarization remains underexplored. To delve into this problem, we construct a UPLight RGB-P segmentation benchmark with 12 typical underwater semantic classes. In this work, we design the ShareCMP, an RGB-P semantic segmentation framework with a shared dual-branch architecture, which reduces the number of parameters by about 26-33% compared to previous dual-branch models. It encompasses a Polarization Generate Attention (PGA) module designed to generate polarization modal images with richer polarization properties for the encoder. In addition, we introduce the Class Polarization-Aware Loss (CPALoss) to improve the learning and understanding of the encoder for polarization modal information and to optimize the PGA module. With extensive experiments on a total of three RGB-P benchmarks, our ShareCMP achieves state-of-the-art performance in mIoU with fewer parameters on the UPLight (92.45(+0.32)%), ZJU (92.7(+0.1)%), and MCubeS (50.99(+1.51%)) datasets compared to the previous best methods. The code is available at <https://github.com/LEFTeyex/ShareCMP>.

1. Introduction

Multimodal semantic segmentation provides the autonomous vehicle with scene understanding capability [13, 54] using perceptual modalities such as RGB-Depth, -Thermal, -Event, and -LiDAR, and is also developing rapidly in recent years. In underwater scenes, Autonomous Underwater Vehicles (AUVs) also need this kind of scene understanding capability to perceive comprehensive environmental information and make correct decisions. Inspired by the use of polarized light by the mantis shrimp to perceive the underwater environment [9, 30], we apply the modality of RGB-Polarization to the perception system of AUVs to improve the perception capability of AUVs in

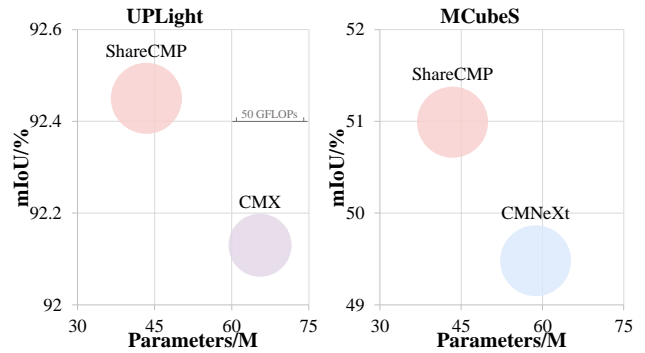


Figure 1. Analysis of our ShareCMP, CMX [45] and CMNeXt [46]. Our ShareCMP outperforms CMX and CMNeXt on the UPLight and MCubeS [25] RGB-P datasets and reduces the number of parameters by about 26-33%.

complex underwater environments.

Most of the current multimodal semantic segmentation methods [24, 34, 47, 52] are designed for RGB-D and RGB-T, and the model designed based on RGB-P also refers to the mainstream methods using the Degree of Linear Polarization (DoLP) or the Angle of Linear Polarization (AoLP) calculated from polarized images as the polarization modal input [1, 21, 25, 37, 40]. However, the polarization properties of polarized images are not further explored. We believe that this fixed paradigm of DoLP and AoLP cannot fully represent the polarization image properties and has certain limitations. Meanwhile, the current mainstream multimodal semantic segmentation methods [24, 45, 46] (RGB-X) adopt a dual-branch architecture to extract features for RGB and X modalities separately and perform attention interaction and fusion for these two modalities. Although these mainstream methods perform well on many multimodal benchmarks, they have two backbone branches and a large number of parameters that are not convenient for model deployment.

To delve into RGB-P multimodal semantic segmentation, we create an underwater RGB-P semantic segmentation benchmark that includes 0, 45, 90, and 135 degree polarized images with a total of 12 classes, which we call

*Corresponding author.

UPLight. In this paper, we investigate the performance of different polarization modalities in multimodal semantic segmentation and design a non-fixed paradigm Polarization Generate Attention (PGA) module using four-angle polarized images to generate better polarization modal images for the RGB-P multimodal semantic segmentation model. While based on the principle that the polarization angles of light reflected by different categories of materials are different, we propose a Class Polarization-Aware Loss (CPALoss) to assist the model in learning the polarization properties of different classes and improve the multimodal feature understanding and interaction capabilities of the RGB-P model. To reduce the number of parameters of the dual-branch model and reduce the resource consumption of model deployment, we design a shared dual-branch multimodal semantic segmentation architecture. Our method is called ShareCMP, which is inspired by CMX [45].

With extensive experiments on UPLight and two additional public RGB-P datasets, we obtain performance evaluations of the ShareCMP model. ShareCMP achieves top mIoU of 92.45(+0.32)% on UPLight, 92.4(+0.2)% (MiT-B2 [39])/92.7(+0.1)% (MiT-B4) on ZJU [37], and 50.34(+1.92)% (RGB-A)/50.55(+16.45)% (RGB-D)/50.99(+1.51)% (RGB-A-D) on MCubeS [25] datasets compared to the previous best methods. Our ShareCMP outperforms all previous RGB-P methods on these three datasets, achieving state-of-the-art performance with fewer parameters.

In conclusion, we deliver the following contributions:

- We construct a new benchmark UPLight for underwater RGB-P semantic segmentation, which provides data support for AUVs to perform special perception tasks.
- We consider the shortcomings of the current dual-branch multimodal model and present a ShareCMP architecture with a shared dual-branch architecture to reduce the number of model parameters.
- We explore and compare different polarization modal representations and propose the PGA module to generate the representation with richer polarization properties.
- CPALoss is proposed, with Class Polarization-Aware Auxiliary Head (CPAAHead) to improve the learning and understanding of the encoder for polarization properties.

2. Related Work

Semantic segmentation. Semantic segmentation can be seen as an extension of image classification from image level to pixel level. Since fully convolutional networks [28] introducing the end-to-end per-pixel classification paradigm, semantic segmentation has advanced significantly. The methods include capturing multi-scale features [4, 5, 16, 49], appending channel and self-attention blocks [7, 12, 18, 42], refining context priors [19, 26, 41,

43], and leveraging edge cues [2, 11, 23, 36]. More recent methods prove the effectiveness of transformer-based architectures for semantic segmentation [35, 38, 39, 50]. While these works achieve high performance, they still suffer under real-world conditions where RGB images do not provide sufficient textures such as low illumination and high dynamic areas.

Multimodal semantic segmentation. At present, multimodal semantic segmentation has been widely studied, such as RGB-Depth [34, 51, 52], RGB-Thermal [13, 24, 47], RGB-Event [44], RGB-LiDAR [55], RGB-Polarization [1, 21, 25, 31, 37, 40], *etc.* These methods adopt dual-branch or multi-branch architectures and use different attention modules between different branches for multi-scale cross-modal information interaction. Recently, unified multimodal segmentation CMX [45] and arbitrary-modal semantic segmentation CMNeXt [46] have achieved better performance. However, the multiple branches of these methods have a large number of parameters, which makes model deployment difficult. Although the single-branch method based on data modal fusion [27] is convenient for model development, its performance is far inferior to the dual-branch model. Therefore, there is an urgent need to develop a multimodal semantic segmentation method that is easy to use and has excellent performance. Among the many data modalities, the polarization modality is quite different from other modalities. Its raw data are RGB images with different polarization angles, which is also a part of the RGB image because the RGB image consists of all polarization angle lights. We believe that the DoLP and AoLP [1, 22] calculated from the raw data cannot fully represent the polarization image properties, which also limits the performance of the RGB-P model. To this end, we propose ShareCMP, a shared dual-branch RGB-P multimodal semantic segmentation framework.

3. Proposed Framework: ShareCMP

3.1. ShareCMP Architecture

ShareCMP consists of a shared dual-branch and four-stage encoder, and its architecture is designed based on CMX [45] and Segformer [39]. Both RGB and polarization modalities are encoded by a shared dual-branch encoder, and the four-stage architecture provides pyramidal fused features to the decoder. Meta-Transformer [48] shows that different modalities can be uniformly encoded using different data-to-sequence tokenization and a shared encoder. Inspired by this, we design a unified encoder with shared parameters for RGB and polarization modalities, as shown in Fig. 2. Each stage of the shared encoder consists of three modules: Overlap Patch Embeddings (OPEmbed), Efficient Self-Attention (ESAttn), and Mix-FFN (MFFN) [39]. OPEmbed generates feature patches with local continuous information. The

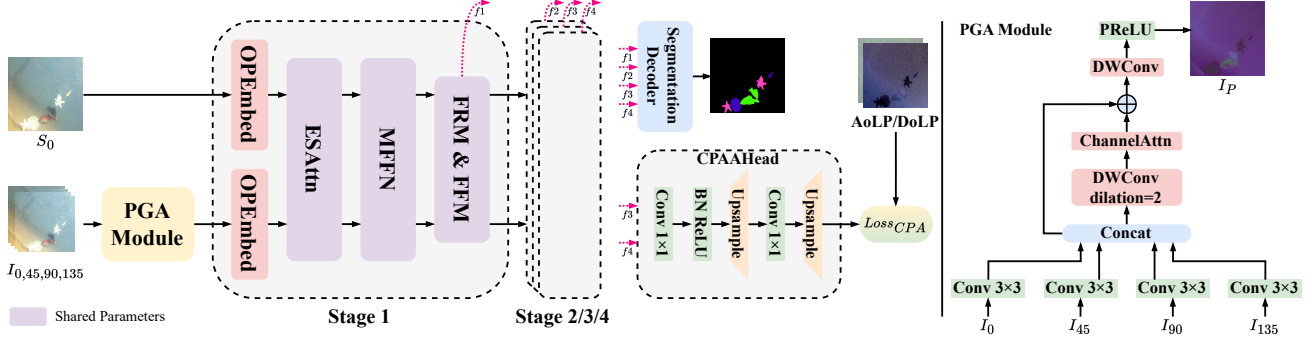


Figure 2. ShareCMP framework. The ShareCMP encoder consists of modules with modal exclusive Overlap Patch Embeddings (OPEmbed) and other shared parameters in each stage. The Polarization Generate Attention (PGA) module generates a polarization modal image input with rich polarization properties based on channel attention and large receptive fields. The Class Polarization-Aware Auxiliary Head (CPAAHead) uses the f_3 and f_4 fused features in the ShareCMP encoder to construct Class Polarization-Aware Loss (CPALoss) $Loss_{CPA}$ to improve the capability of the encoder to perceive optical polarization properties of different classes and optimize the PGA module.

feature patches are forwarded to the following ESAttn and MFFN modules. At each stage, the modal exclusive OPEmbed (ME OPEmbed) is constructed for the input x_{RGB} and x_P , respectively, and using the shared-parameters ESAttn and MFFN introduces self-attention and leak location information [39] to obtain y_{RGB} and y_P .

$$y_{RGB}^{patch} = \text{OPEmbed}_{RGB}(x_{RGB}) \quad (1)$$

$$y_P^{patch} = \text{OPEmbed}_P(x_P) \quad (2)$$

$$y_{RGB} = \text{MFFN}(\text{ESAttn}(y_{RGB}^{patch})) \quad (3)$$

$$y_P = \text{MFFN}(\text{ESAttn}(y_P^{patch})) \quad (4)$$

where y_X^{patch} is feature patches of x_X . After that, the Feature Rectification Module (FRM) and the Feature Fusion Module (FFM) [45] introduce multimodal cross-attention for y_{RGB} and y_P and fuse their feature information. After the encoder, the four-stage fused features $f_i \in \{f_1, f_2, f_3, f_4\}$ are forwarded to the MLP decoder [39] for the segmentation prediction. We also refer to the shared dual-branch encoder (ShareCMP encoder) as the pseudo-single-branch encoder. Although it still retains the dual-branch inference architecture, it reduces the number of multimodal encoder parameters by about 30%.

3.2. Polarization Generate Attention Module

To better represent the properties of polarization modal data, we develop the Polarization Generate Attention (PGA) module to generate polarization modal information with more polarization properties to better serve downstream tasks as semantic segmentation. As shown in Fig. 2, PGA uses Convolution (Conv) with 3×3 kernel size for four input images with 0, 45, 90, and 135 polarization angles $\{I_a | a \in \{0, 45, 90, 135\}, I_a \in H \times W\}$ to extract features and increases the receptive field of features without reduc-

ing the resolution of the image features. Finally, the concatenated feature $f_P \in H \times W$ is obtained, as in Eq. (5).

$$f_P = \text{Concat}(\text{Conv}_{3 \times 3}(I_0), \text{Conv}_{3 \times 3}(I_{45}), \text{Conv}_{3 \times 3}(I_{90}), \text{Conv}_{3 \times 3}(I_{135})) \quad (5)$$

Previous multimodal fusion methods indicate channel information is crucial [6, 17]. Inspired by this, after obtaining the concatenated feature f_P , using Depth-Wise Convolution (DWConv), which consists of convolution with 1×1 kernel size and with 3×3 kernel size composed of grouped convolution with 2 dilation [27], provides the following channel attention module with advanced features with a larger receptive field to enhance the generated channel attention features Attn_P . The processing can be formalized as:

$$\text{Attn}_P = \text{ChannelAttn}(\text{DWConv}_{dila=2}(f_P)) \quad (6)$$

Finally, the concatenated feature f_P is computed by attention, residual connection, feed-forward network composed of DWConv and PReLU [15] activation, then the three-channel polarization modal image $I_P \in H \times W$ is generated. It can be formalized as:

$$I_P = \text{PReLU}(\text{DWConv}(f_P + \text{Attn}_P * f_P)) \quad (7)$$

The activation function is PReLU in PGA to improve performance [27]. And PGA is a lightweight module with a simple architecture.

3.3. Class Polarization-Aware Loss

To improve the learning and understanding of the encoder for polarization modal information, we design the Class Polarization-Aware Loss (CPALoss) and build the corresponding Class Polarization-Aware Auxiliary Head (CPAAHead) for CPALoss, as illustrated in Fig. 2. Based on the

principle that the reflected light from different categories of materials produces different degrees of polarization and angles of polarization, CPALoss uses the estimates of AoLP and DoLP corresponding to different classes generated by CPAAHead and the ground truth AoLP and DoLP calculated from polarized images at four angles of 0, 45, 90, and 135 to calculate the loss $Loss_{CPA}$. The loss is optimized to improve the capability of the encoder for perceiving the optical polarization properties of different classes while improving the quality of the polarization modal image generated by the PGA module. CPAAHead, which has a similar architecture to the MLP decoder [39], uses the multi-scale multimodal fusion features generated in the encoder to estimate the AoLP and DoLP of different classes in the image, respectively. CPAAHead constructs two convolution layers with 1×1 kernel size for each scale feature. Upsampling operations are performed after the first convolution layer and the second convolution layer to unify the different scales of the features and to align the estimation and ground truth size of the AoLP or DoLP. The CPALoss can be written as:

$$\hat{A}_i / \hat{D}_i = \text{Conv}_{1 \times 1}^{up}(\text{Conv}_{1 \times 1}^{up}(\mathbf{f}_i)) \quad (8)$$

$$Loss_{CPA} = \lambda \sum_i^{Sta} \sum_c^{Cls} ((\mathbf{A}_i^c - \hat{\mathbf{A}}_i^c)^2 + (\mathbf{D}_i^c - \hat{\mathbf{D}}_i^c)^2) \quad (9)$$

where $i \in Sta\{1, 2, 3, 4\}$ represents the index of the i stage in the encoder, $c \in Cls$ represents the class in the dataset. $\text{Conv}_{1 \times 1}^{up}$ is a convolution with 1×1 followed by upsampling. $\hat{\mathbf{A}}/\hat{\mathbf{D}}$, \mathbf{A}/\mathbf{D} are the estimation and ground truth of AoLP/DoLP, respectively. λ is the loss weight of CPALoss, which we set to 0.01 after experiments. We set CPALoss at 3 and 4 stages, more detailed analysis in Sec. 4.3.

4. Experiments

4.1. Polarization Modal Representations

Polarization is a basic property of light, expressing the direction of light vibration. The vibration of polarized light has a fixed direction or a regular change of direction and is classified as linearly polarized light, circularly polarized light, and elliptically polarized light. The polarization sensor is usually set four polarization plates with different angles ($0^\circ, 45^\circ, 90^\circ, 135^\circ$) on every four pixels, which collects linearly polarized images $\{\mathbf{I}_0, \mathbf{I}_{45}, \mathbf{I}_{90}, \mathbf{I}_{135}\}$ with pixels aligned at these four angles at the same time. We investigate four polarization modal representations [1, 37], the Angle of Linear Polarization (AoLP), the Degree of Linear Polarization (DoLP), the Sin Angle of Linear Polarization (SAoLP), and the Cos Angle of Linear Polarization (CAoLP), which the SAoLP and the CAoLP are designed based on the principles of trigonometric functions. These polarization modal representations are derived from stokes vectors $\mathbf{S} = \{S_0, S_1, S_2, S_3\}$ that describe the polarization

state of the light. Precisely, S_0 represents the total light intensity, S_1 and S_2 denote the ratio of 0° and 45° linear polarization over its perpendicular polarized portion, and S_3 stands for the circular polarization power which is not involved in our work. The stokes vectors \mathbf{S} can be calculated by the following Eq. (10).

$$\mathbf{S} = \begin{cases} S_0 = \mathbf{I}_0 + \mathbf{I}_{90} = \mathbf{I}_{45} + \mathbf{I}_{135} \\ S_1 = \mathbf{I}_0 - \mathbf{I}_{90} \\ S_2 = \mathbf{I}_{45} - \mathbf{I}_{135} \end{cases} \quad (10)$$

In the work, to represent the total light intensity more accurately, we use Eq. (11) to calculate S_0 [1, 22], and make S_0 be the RGB input image of the RGB-P multimodal semantic segmentation model.

$$S_0 = (\mathbf{I}_0 + \mathbf{I}_{90} + \mathbf{I}_{45} + \mathbf{I}_{135})/2 \quad (11)$$

Then, AoLP, DoLP, SAoLP, and CAoLP are formally computed as follows:

$$AoLP = \frac{1}{2} \arctan\left(\frac{S_2}{S_1}\right) \quad (12)$$

$$DoLP = \frac{\sqrt{S_1^2 + S_2^2}}{S_0} \quad (13)$$

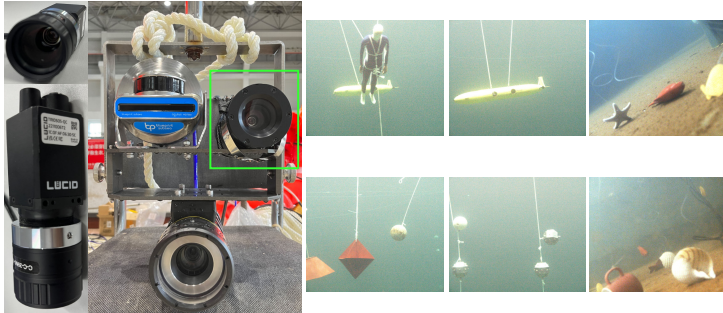
$$SAoLP = \frac{1}{2} \arcsin\left(\frac{S_2}{S_0}\right) \quad (14)$$

$$CAoLP = \frac{1}{2} \arccos\left(\frac{S_1}{S_0}\right) \quad (15)$$

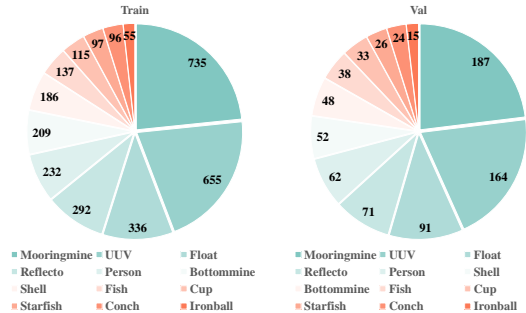
In our experiments, we further studied the impact of AoLP, DoLP, SAoLP, and CAoLP on the performance of RGB-P multimodal semantic segmentation. We use AoLP, DoLP, SAoLP, and CAoLP as inputs to the polarization modality of the RGB-P model, respectively, to analyze the differences between them.

4.2. Datasets and Implementation Details

UPLight dataset is an underwater RGB-P semantic segmentation dataset that we create for AUV perception, which has 12 classes. We use a LUCID_TRI050S-QC polarization sensor with a C-C-39N0-160-R12 liquid lens and customize a waterproof housing for underwater use, as the green box in Fig. 3a (the sonar on the left side of the polarization sensor and another camera below are used for other tasks, which are not related to this work). We mainly collect color polarized images of typical underwater objects arranged in the pool to provide data support for AUV to perform special perception tasks. Detailed dataset information is as shown in Fig. 3. The dataset is split into 1441/350 image pairs for training/validation at the size of 1224×1024 . Each image pair includes four polarized images with different polarization angles ($0^\circ, 45^\circ, 90^\circ, 135^\circ$). The input image is resized to 612×512 .



(a) Collecting device and images of the UPLight.



(b) Distribution of object quantity in 12 semantic classes.

Figure 3. UPLight RGB-P multimodal dataset.

ShareCMP	Stage				mIoU \uparrow
	1	2	3	4	
w/ ME OPEmbed	✓				91.91
w/ ME OPEmbed	✓	✓			92.36
w/ ME OPEmbed	✓	✓	✓		92.01
w/ ME OPEmbed	✓	✓	✓	✓	92.45

Table 1. Ablation study of modal exclusive OPEmbed (ME OPEmbed) on different encoder stages.

ZJU dataset [37] is an RGB-P multimodal dataset for automated driving on complex campus street scenes, which has 8 classes. It has 344/50 image pairs for training/validation at the size of 1224×1024 . Each image pair includes four polarized images with different polarization angles ($0^\circ, 45^\circ, 90^\circ, 135^\circ$). The input image is resized to 612×512 .

MCubeS dataset [25] is an RGB-P-NIR multimodal dataset for material segmentation on different street scenes, which has 20 classes. It has 302/96/102 image pairs for training/validation/test at the size of 1224×1024 . Each image pair includes RGB, AoLP, DoLP, and Near-Infrared (NIR) images. The input image is resized to 612×512 .

Implementation details. Our implementations are based on the MMsegmentation toolbox [8]. Unless otherwise specified, we train our models on 2 A6000 GPUs with an initial learning rate (LR) of $6e^{-5}$, which is scheduled by the poly strategy with power 1.0 over 200 epochs. The first 5 epochs are to warm up models with $1e^{-6} \times$ the initial LR. The optimizer is AdamW [29] with a weight decay of 0.01, and the batch size is 4 per GPU. We use cross-entropy as the semantic segmentation loss function. The images are augmented by random resize with a ratio of 0.5-2.0, random horizontal flipping, random color jitter, and random cropping to 612×512 on all datasets. To conduct comparisons, the ImageNet-1K [10] pre-trained weight is used for ShareCMP on all datasets, but not for OPEmbed [39]

ShareCMP	Stage				mIoU \uparrow
	1	2	3	4	
w/ CPALoss	✓	✓	✓	✓	91.79
w/ CPALoss		✓	✓	✓	91.63
w/ CPALoss			✓	✓	92.45
w/ CPALoss				✓	91.72

Table 2. Ablation study of the CPALoss.

modules in the polarization modal branch. We use mean Intersection over Union (mIoU) averaged across semantic classes as the primary evaluation metric to measure the segmentation performance.

4.3. Ablation Study

Ablation of ShareCMP encoder. The ablation of setting non-shared parameters modal exclusive OPEmbed [39] on different stages of ShareCMP encoder is conducted, as shown in Tab. 1. When the ShareCMP encoder sets modal exclusive OPEmbed in stage 1, its encoder architecture is similar to that of the Meta-Transformer unified encoder [48], but it has poor performance. We believe that ShareCMP has multimodal attention interaction operations (by FRM and FFM [45]) after each stage. Simply setting a modal exclusive OPEmbed in stage 1 cannot meet the generalization performance requirements of the ShareCMP encoder. ShareCMP achieves the best performance when modal exclusive OPEmbed is set in all encoder stages.

Ablation of CPALoss. As shown in Tab. 2, we ablate the combination of CPALoss used in different ShareCMP encoder stages and require that deep and high-level features must be optimized for CPALoss. When the CPALoss is optimized in stages 3 and 4, ShareCMP achieves the best performance.

Ablation of ShareCMP. In Tab. 4, we show the semantic segmentation performance of ShareCMP without CPALoss

Method	Modal	Unlabeled	Mooringmine	UUV	Float	Reflector	Person	Bottommine	Cup	Ironball	Conch	Fish	Shell	Starfish	mIoU \uparrow
SegFormer-B2 [39]	RGB	99.49	92.77	94.47	89.12	97.96	95.00	97.44	89.66	82.92	84.12	89.31	83.25	69.25	89.60
MCubeSNet [25]	RGB-AoLP	89.72	83.32	84.78	85.20	88.79	85.63	88.94	81.76	75.47	83.37	80.77	81.40	65.18	82.64
EAFNet [37]	RGB-AoLP	94.61	88.21	89.67	90.09	93.68	90.52	93.83	86.65	80.36	88.26	85.66	86.29	70.07	87.53
CMX (MiT-B2) [45]	RGB-AoLP	99.53	93.08	94.90	92.27	98.07	95.27	97.88	88.67	84.83	93.60	90.40	92.62	76.53	92.13
MCubeSNet	RGB-DoLP	87.88	81.48	82.94	83.36	86.95	83.79	87.10	79.92	73.63	81.53	78.93	79.56	63.34	80.80
EAFNet	RGB-DoLP	94.42	88.02	89.48	89.90	93.49	90.33	93.64	86.46	80.17	88.07	85.47	86.10	69.88	87.34
CMX (MiT-B2)	RGB-DoLP	99.53	92.88	94.79	90.48	98.19	95.22	97.51	92.00	85.48	91.26	90.95	92.51	76.17	92.07
ShareCMP (MiT-B2)	RGB- $\{I_0, I_{45}, I_{90}, I_{135}\}$	99.53	93.13	94.59	95.01	98.60	95.44	98.75	91.57	85.28	93.18	90.58	91.21	74.99	92.45

Table 3. Results on UPLight.

Method	Modal	mIoU \uparrow
ShareCMP	RGB- $\{I_0, I_{45}, I_{90}, I_{135}\}$	92.45
w/o CPALoss	RGB- $\{I_0, I_{45}, I_{90}, I_{135}\}$	91.09(-1.36)
w/o PGA	RGB-AoLP	91.96(-0.49)
w/o PGA	RGB-DoLP	92.03(-0.42)
w/o PGA	RGB-SAoLP	90.63(-1.82)
w/o PGA	RGB-CAoLP	91.15(-1.30)

Table 4. Ablation study of the ShareCMP framework.

or PGA and investigate the effect of the four polarization modalities AoLP, DoLP, SAoLP, and CAoLP on the RGB-P semantic segmentation performance. When removing the CPALoss for polarization-aware learning, the performance decreases significantly by 1.36%. Our designed SAoLP and CAoLP, which are new representation methods for the polarization modality, result in poor performance decreases of 1.82% and 1.30%, respectively. Since SAoLP and CAoLP are part of AoLP, their polarization modal representation is not as complete as AoLP, resulting in reduced performance. While AoLP and DoLP result in a similar slight decrease in performance, it indicates that AoLP and DoLP have similar effects on the ShareCMP and are also relatively effective polarization modal representations. Regardless of the fixed paradigm of the polarization modal representation, its performance is not as good as the representation generated by our PGA. The results confirm that our CPALoss and PGA are more advantageous for RGB-P semantic segmentation.

4.4. Comparison against the State of the Art

To verify the efficacy of our proposed ShareCMP framework, we perform extensive experiments on three RGB-P segmentation datasets. The results and comparisons against the state-of-the-art are shown in Tabs. 3, 5 and 6.

Results on UPLight. As shown in Tab. 3, we train models [25, 37, 45] that can be used for RGB-P semantic segmentation and compare them with ShareCMP on the UP-

Light dataset we built. Our ShareCMP achieves the best performance of 92.45%. Compared to the RGB-only baseline with SegFormer-B2 [39], the IoU improvements on classes with polarization properties are clear, such as Float (+5.9%), Bottom mine (+1.3%), Ironball (+2.4%), Conch (+9.1%), Shell (+8.0%), and Starfish (+5.7%). This also shows that our RGB-P multimodal semantic segmentation model ShareCMP has important application significance in underwater aquaculture, fishing, ocean exploration, *etc.* ShareCMP has only about 65% of the number of parameters of CMX [45] (detailed parameter number analysis in Sec. 4.5), and has a 0.32% performance improvement compared to CMX, which provides more advantages in the deployment of ShareCMP and its performance improvement on AUVs.

Results on ZJU. In Tab. 5, we perform experiments to compare the ShareCMP method with the previous state-of-the-art methods [32, 37, 40, 45] on the ZJU [37] dataset. Our ShareCMP outperforms the previous best RGB-P method by 0.2% and 0.1% based on MiT-B2 [39] and MiT-B4, respectively. Compared to dual-branch multimodal semantic segmentation models [37, 40, 45], our ShareCMP beats them in segmentation performance with only about 65% of their parameters.

Results on MCubeS. In Tab. 6, we benchmark 7 semantic segmentation methods on the MCubeS [25] dataset, which contains AoLP, DoLP, and NIR modalities. Since the MCubeS dataset does not provide corresponding four-angle polarized images, our ShareCMP uses AoLP and DoLP as polarization modal inputs. On RGB-A and RGB-D modal inputs, our ShareCMP outperforms the previous best method by 1.92% on CMNeXt [46] and 16.45% on MCubeSNet [25]. ShareCMP achieves a state-of-the-art performance of 50.99% when concatenating AoLP and DoLP modalities. In addition, our ShareCMP (RGB-A-D) even outperforms previous methods [3, 14, 20, 25, 33, 53] using RGB-A-D-N modalities, by 8.09% compared to the best. The results indicate that our ShareCMP has great po-

Method	Modal	Building	Glass	Car	Road	Tree	Sky	Pedestrian	Bicycle	mIoU \uparrow
SwiftNet [32]	RGB	83.0	73.4	91.6	96.7	94.5	84.7	36.1	82.5	80.3
SegFormer-B2 [39]	RGB	90.6	79.0	92.8	96.6	96.2	89.6	82.9	89.3	89.6
NLFNet [40]	RGB-AoLP	85.4	77.1	93.5	97.7	93.2	85.9	56.9	85.5	84.4
EAFNet [37]	RGB-AoLP	87.0	79.3	93.6	97.4	95.3	87.1	60.4	85.6	85.7
EAFNet	RGB-DoLP	86.4	76.9	93.0	97.1	95.5	86.1	62.1	86.0	85.4
CMX (MiT-B2) [45]	RGB-AoLP	91.5	87.3	95.8	98.2	96.6	89.3	85.6	91.9	92.0
CMX (MiT-B2)	RGB-DoLP	91.8	87.8	96.1	98.2	96.7	89.4	86.1	91.8	92.2
ShareCMP (MiT-B2)	RGB- $\{I_0, I_{45}, I_{90}, I_{135}\}$	91.4	88.4	96.2	98.2	96.7	90.2	85.7	92.2	92.4
CMX (MiT-B4)	RGB-AoLP	91.6	88.8	96.3	98.3	96.8	89.7	86.2	92.8	92.6
CMX (MiT-B4)	RGB-DoLP	91.6	88.6	96.3	98.3	96.7	89.5	86.4	92.2	92.5
ShareCMP (MiT-B4)	RGB- $\{I_0, I_{45}, I_{90}, I_{135}\}$	92.0	88.6	96.3	98.3	96.8	90.0	87.2	92.5	92.7

Table 5. Results on ZJU [37]. ShareCMP is trained for 500 epochs.

Method	Modal	Asphalt	Concrete	Metal	RoadMa	Fabric	Glass	Plaster	Plastic	Rubber	Sand	Gravel	Ceramic	Cobbles	Brick	Grass	Wood	Leaf	Water	Sky	mIoU \uparrow	
DRConv [3]	RGB-A-D-N	-	-	-	-	-	-	-	-	-	-	-	-	-	-	-	-	-	-	-	-	34.63
DDF [53]	RGB-A-D-N	-	-	-	-	-	-	-	-	-	-	-	-	-	-	-	-	-	-	-	-	36.16
TransFuser [33]	RGB-A-D-N	-	-	-	-	-	-	-	-	-	-	-	-	-	-	-	-	-	-	-	-	37.66
MMTM [20]	RGB-A-D-N	-	-	-	-	-	-	-	-	-	-	-	-	-	-	-	-	-	-	-	-	39.71
FuseNet [14]	RGB-A-D-N	-	-	-	-	-	-	-	-	-	-	-	-	-	-	-	-	-	-	-	-	40.58
MCubeSNet [25]	RGB-A-D-N	85.7	42.6	47.0	59.2	12.5	44.3	3.0	10.6	12.7	66.8	67.1	27.8	65.8	36.8	54.8	39.4	73.0	13.3	94.8	42.90	
MCubeSNet	RGB-A	83.3	42.3	43.0	58.4	8.8	27.3	0.6	9.8	12.0	55.5	57.7	18.1	64.6	36.6	56.5	34.8	71.8	6.8	95.0	39.10	
CMNeXt (MiT-B2) [46]	RGB-A	-	-	-	-	-	-	-	-	-	-	-	-	-	-	-	-	-	-	-	-	48.42
ShareCMP (MiT-B2)	RGB-A	88.2	49.3	51.0	66.1	20.7	50.1	1.2	30.9	18.2	64.2	75.2	28.5	74.9	45.7	59.4	43.9	74.1	69.9	95.6	50.34	
MCubeSNet	RGB-D	75.2	40.2	37.8	53.9	4.2	32.3	1.9	14.3	11.3	59.7	21.8	11.6	28.9	29.1	54.6	29.4	71.4	9.6	94.3	34.10	
ShareCMP (MiT-B2)	RGB-D	88.5	50.4	52.6	65.9	23.2	49.8	0.0	36.7	18.8	64.6	75.4	30.4	72.2	45.3	57.3	43.9	74.5	66.1	95.7	50.55	
MCubeSNet	RGB-A-D	83.0	42.6	45.5	59.8	17.0	44.2	1.2	18.6	4.8	54.8	51.5	26.4	67.6	41.9	57.0	39.4	74.0	15.5	95.3	42.00	
CMNeXt (MiT-B2)	RGB-A-D	-	-	-	-	-	-	-	-	-	-	-	-	-	-	-	-	-	-	-	-	49.48
ShareCMP (MiT-B2)	RGB-A-D	88.8	49.7	52.5	66.4	27.6	51.0	0.2	31.5	18.0	69.9	79.0	30.9	71.4	42.8	58.3	44.1	74.5	67.6	95.6	50.99	

Table 6. Results on MCubeS [25]. The human body class is omitted as its result is 0%.

tential in RGB-P multimodal semantic segmentation.

4.5. Quantitative and Visual Analysis

Quantitative analysis of ShareCMP. In Tab. 7, our ShareCMP reduces the number of parameters by 22.12 M compared to CMX [45], while the number of parameters of the ShareCMP encoder is only 65.7% of the CMX encoder. Compared to CMNeXt [46], our ShareCMP also significantly reduces the number of parameters while increasing the computational complexity by only 0.77 G FLOPs. Compared to these state-of-the-art methods, our ShareCMP reduces a large number of parameters while still improving the segmentation performance, which also proves the efficacy of our proposed ShareCMP framework.

Visualization of polarization modal representations. We show five polarization modal representations, as in Fig. 4. Compared with SAoLP and CAoLP, AoLP and DoLP cover the polarization information in SAoLP and CAoLP and show richer polarization features, which also verifies that the segmentation results of RGB-AoLP and RGB-DoLP are better than RGB-SAoLP and RGB-CAoLP in Tab. 4. While

Structure	#Params(M) \downarrow	FLOPs(G) \downarrow
CMX [45]	65.52	52.03
- Encoder	64.98	47.07
ShareCMP	43.40 (-22.12)	66.19(+14.16)
- Encoder	42.72 (-22.26)	46.71
- PGA	0.16	14.53
CMNeXt [46]	58.73	65.42

Table 7. Comparison of the number of parameters (#Params) and FLOPs which are counted in 512×512 .

I_P has rich polarization properties, it also provides different color features for objects with different polarization properties, such as the glass reflection and the reflector of the motorcycle, the car shell at different angles in the second group of images, the glass and the sticker on the car glass on the right side, and different colors of classes in the third and fourth groups of images. The AoLP and SAoLP in the third group of images only have very few polarization features,

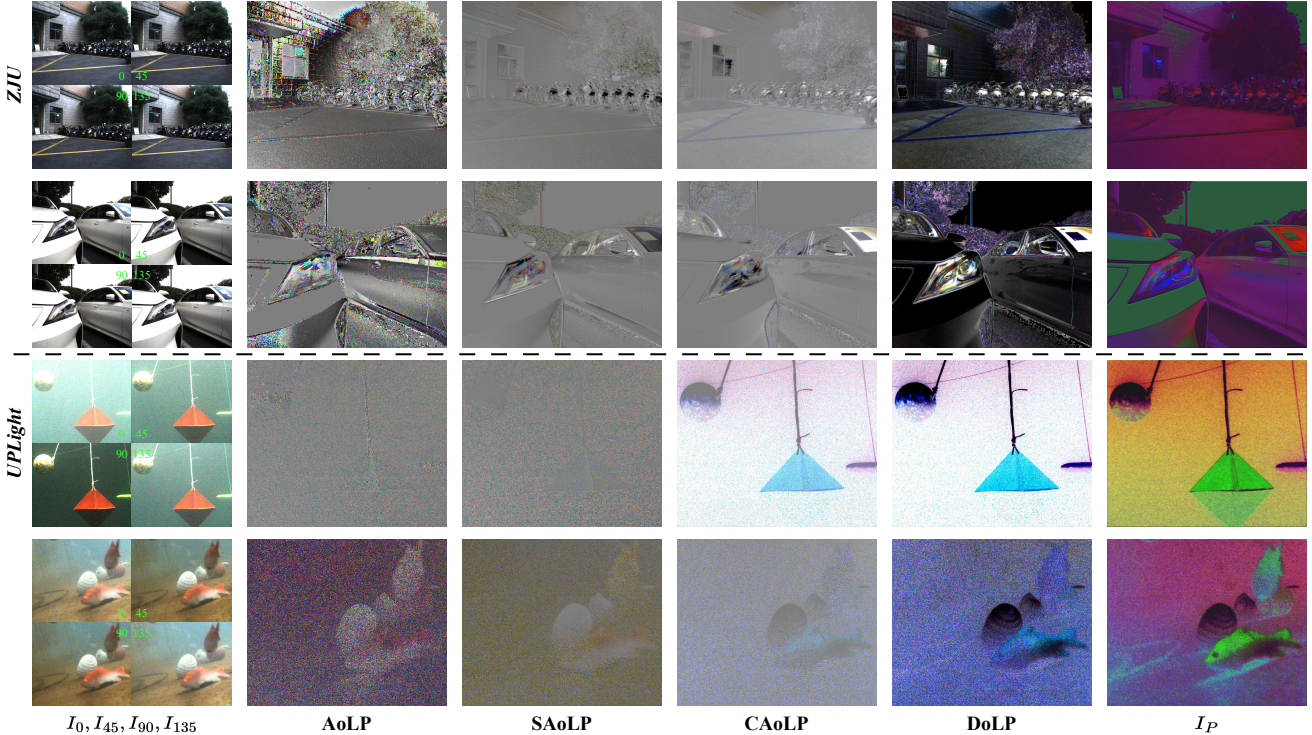


Figure 4. Visualization of different polarization modal representations.

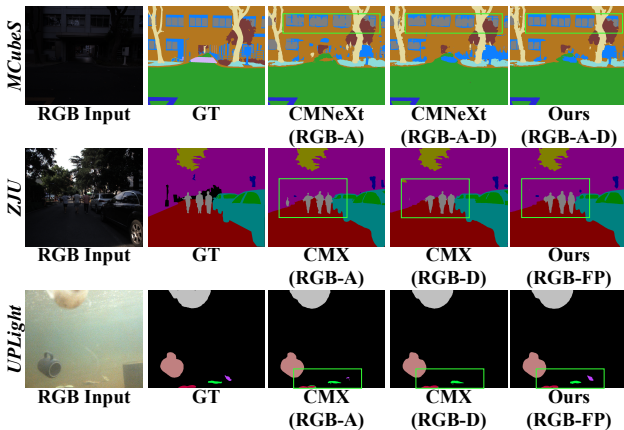


Figure 5. Visualization of segmentation results. RGB-FP represents RGB and four polarized images with different polarization angles (RGB- $\{I_0, I_{45}, I_{90}, I_{135}\}$).

while our I_P can still provide rich polarization features, indicating that our PGA module has good robustness in generating polarization features. In addition, compared to I_P , the other four polarization modal representations are very coarse in some areas and have a lot of noise points, while I_P has smoother polarization features that eliminate a large number of noise points, especially for the underwater polarization modal representations in the UPLight dataset.

Visualization of segmentation results. In Fig. 5, we show the semantic segmentation results of our ShareCMP against the CMX [45] with RGB-A and RGB-D and the CMNeXt [46] with RGB-A and RGB-A-D. It can be seen that our ShareCMP achieves a more complete segmentation for glass windows on MCubeS [25] and persons on ZJU [37] images, all in the case of insufficient illumination. For blurred underwater images in UPLight, CMX does not segment the starfish in the image or segments the starfish and shells incompletely. Our ShareCMP is more robust in underwater scenes and accurately segments all objects.

5. Conclusion

In this work, to revitalize multimodal pixel-wise semantic scene understanding for Autonomous Underwater Vehicles (AUVs), we investigate RGB-P semantic segmentation and propose ShareCMP, a shared dual-branch architecture, which reduces a large number of model parameters. We put forward the UPLight RGB-P multimodal dataset with 12 typical underwater semantic classes. We propose the Polarization Generate Attention (PGA) module, which can stably generate polarization modal images with rich polarization properties. The designed Class Polarization-Aware Loss (CPALoss) improves the learning and understanding of the encoder for polarization modal information. Our ShareCMP achieves state-of-the-art performance with fewer parameters on three RGB-P datasets.

Acknowledgment. This research is funded by the National Natural Science Foundation of China, grant number 52371350, by the Natural Science Foundation of Hainan Province, grant number 2021JJLH0002, by the Foundation of National Key Laboratory, grant number JCKYS2022SXJQR-06, and 2021JCJQ-SYSJJ-LB06912.

References

- [1] Michael Baltaxe, Tomer Pe’er, and Dan Levi. Polarimetric imaging for perception. *arXiv preprint arXiv:2305.14787*, 2023. 1, 2, 4
- [2] Shubhankar Borse, Ying Wang, Yizhe Zhang, and Fatih Porikli. Inverseform: A loss function for structured boundary-aware segmentation. In *CVPR*, pages 5901–5911, 2021. 2
- [3] Jin Chen, Xijun Wang, Zichao Guo, Xiangyu Zhang, and Jian Sun. Dynamic region-aware convolution. In *CVPR*, pages 8064–8073, 2021. 6, 7
- [4] Liang-Chieh Chen, George Papandreou, Iasonas Kokkinos, Kevin Murphy, and Alan L Yuille. Deeplab: Semantic image segmentation with deep convolutional nets, atrous convolution, and fully connected crfs. *IEEE TPAMI*, 40(4):834–848, 2017. 2
- [5] Liang-Chieh Chen, Yukun Zhu, George Papandreou, Florian Schroff, and Hartwig Adam. Encoder-decoder with atrous separable convolution for semantic image segmentation. In *ECCV*, pages 801–818, 2018. 2
- [6] Xiaokang Chen, Kwan-Yee Lin, Jingbo Wang, Wayne Wu, Chen Qian, Hongsheng Li, and Gang Zeng. Bi-directional cross-modality feature propagation with separation-and-aggregation gate for rgb-d semantic segmentation. In *ECCV*, pages 561–577, 2020. 3
- [7] Sungha Choi, Joanne T Kim, and Jaegul Choo. Cars can’t fly up in the sky: Improving urban-scene segmentation via height-driven attention networks. In *CVPR*, pages 9373–9383, 2020. 2
- [8] MMSegmentation Contributors. Mmsegmentation: Openmmlab semantic segmentation toolbox and benchmark, 2020. <https://github.com/open-mmlab/msegmentation>. 5
- [9] Ilse M Daly, Martin J How, Julian C Partridge, Shelby E Temple, N Justin Marshall, Thomas W Cronin, and Nicholas W Roberts. Dynamic polarization vision in mantis shrimps. *Nature Communications*, 7(1):12140, 2016. 1
- [10] Jia Deng, Wei Dong, Richard Socher, Li-Jia Li, Kai Li, and Li Fei-Fei. Imagenet: A large-scale hierarchical image database. In *CVPR*, pages 248–255, 2009. 5
- [11] Henghui Ding, Xudong Jiang, Ai Qun Liu, Nadia Magnenat Thalmann, and Gang Wang. Boundary-aware feature propagation for scene segmentation. In *ICCV*, pages 6819–6829, 2019. 2
- [12] Jun Fu, Jing Liu, Haijie Tian, Yong Li, Yongjun Bao, Zhiwei Fang, and Hanqing Lu. Dual attention network for scene segmentation. In *CVPR*, pages 3146–3154, 2019. 2
- [13] Qishen Ha, Kohei Watanabe, Takumi Karasawa, Yoshitaka Ushiku, and Tatsuya Harada. Mfnet: Towards real-time semantic segmentation for autonomous vehicles with multi-spectral scenes. In *IEEE IROS*, pages 5108–5115, 2017. 1, 2
- [14] Caner Hazirbas, Lingni Ma, Csaba Domokos, and Daniel Cremers. Fusernet: Incorporating depth into semantic segmentation via fusion-based cnn architecture. In *ACCV*, pages 213–228, 2017. 6, 7
- [15] Kaiming He, Xiangyu Zhang, Shaoqing Ren, and Jian Sun. Delving deep into rectifiers: Surpassing human-level performance on imagenet classification. In *ICCV*, pages 1026–1034, 2015. 3
- [16] Qibin Hou, Li Zhang, Ming-Ming Cheng, and Jiashi Feng. Strip pooling: Rethinking spatial pooling for scene parsing. In *CVPR*, pages 4003–4012, 2020. 2
- [17] Xinxin Hu, Kailun Yang, Lei Fei, and Kaiwei Wang. Acnet: Attention based network to exploit complementary features for rgbd semantic segmentation. In *ICIP*, pages 1440–1444, 2019. 3
- [18] Zilong Huang, Xinggang Wang, Lichao Huang, Chang Huang, Yunchao Wei, and Wenyu Liu. Ccnet: Criss-cross attention for semantic segmentation. In *ICCV*, pages 603–612, 2019. 2
- [19] Zhenchao Jin, Tao Gong, Dongdong Yu, Qi Chu, Jian Wang, Changhu Wang, and Jie Shao. Mining contextual information beyond image for semantic segmentation. In *ICCV*, pages 7231–7241, 2021. 2
- [20] Hamid Reza Vaezi Joze, Amirreza Shaban, Michael L Iuzolino, and Kazuhito Koishida. Mmtm: Multimodal transfer module for cnn fusion. In *CVPR*, pages 13289–13299, 2020. 6, 7
- [21] Agastya Kalra, Vage Taamazyan, Supreeth Krishna Rao, Kartik Venkataraman, Ramesh Raskar, and Achuta Kadambi. Deep polarization cues for transparent object segmentation. In *CVPR*, pages 8602–8611, 2020. 1, 2
- [22] Chenyang Lei, Chenyang Qi, Jiaxin Xie, Na Fan, Vladlen Koltun, and Qifeng Chen. Shape from polarization for complex scenes in the wild. In *CVPR*, pages 12632–12641, 2022. 2, 4
- [23] Xiangtai Li, Xia Li, Li Zhang, Guangliang Cheng, Jianping Shi, Zhouchen Lin, Shaohua Tan, and Yunhai Tong. Improving semantic segmentation via decoupled body and edge supervision. In *ECCV*, pages 435–452, 2020. 2
- [24] Mingjian Liang, Junjie Hu, Chenyu Bao, Hua Feng, Fuqin Deng, and Tin Lun Lam. Explicit attention-enhanced fusion for rgb-thermal perception tasks. *IEEE RAL*, 2023. 1, 2
- [25] Yupeng Liang, Ryosuke Wakaki, Shohei Nobuhara, and Ko Nishino. Multimodal material segmentation. In *CVPR*, pages 19800–19808, 2022. 1, 2, 5, 6, 7, 8
- [26] Guosheng Lin, Anton Milan, Chunhua Shen, and Ian Reid. Refinenet: Multi-path refinement networks for high-resolution semantic segmentation. In *CVPR*, pages 1925–1934, 2017. 2
- [27] Jinyuan Liu, Zhu Liu, Guanyao Wu, Long Ma, Risheng Liu, Wei Zhong, Zhongxuan Luo, and Xin Fan. Multi-interactive feature learning and a full-time multi-modality benchmark for image fusion and segmentation. In *ICCV*, pages 8115–8124, 2023. 2, 3

- [28] Jonathan Long, Evan Shelhamer, and Trevor Darrell. Fully convolutional networks for semantic segmentation. In *CVPR*, pages 3431–3440, 2015. 2
- [29] Ilya Loshchilov and Frank Hutter. Decoupled weight decay regularization. In *ICLR*, 2019. 5
- [30] N Justin Marshall. A unique colour and polarization vision system in mantis shrimps. *Nature*, 333(6173):557–560, 1988. 1
- [31] Haiyang Mei, Bo Dong, Wen Dong, Jiayi Yang, Seung-Hwan Baek, Felix Heide, Pieter Peers, Xiaopeng Wei, and Xin Yang. Glass segmentation using intensity and spectral polarization cues. In *CVPR*, pages 12622–12631, 2022. 2
- [32] Marin Orsic, Ivan Kreso, Petra Bevandic, and Sinisa Segvic. In defense of pre-trained imagenet architectures for real-time semantic segmentation of road-driving images. In *CVPR*, pages 12607–12616, 2019. 6, 7
- [33] Aditya Prakash, Kashyap Chitta, and Andreas Geiger. Multi-modal fusion transformer for end-to-end autonomous driving. In *CVPR*, pages 7077–7087, 2021. 6, 7
- [34] Yeqiang Qian, Liuyuan Deng, Tianyi Li, Chunxiang Wang, and Ming Yang. Gated-residual block for semantic segmentation using rgb-d data. *IEEE TITS*, 23(8):11836–11844, 2021. 1, 2
- [35] Robin Strudel, Ricardo Garcia, Ivan Laptev, and Cordelia Schmid. Segmenter: Transformer for semantic segmentation. In *ICCV*, pages 7262–7272, 2021. 2
- [36] Towaki Takikawa, David Acuna, Varun Jampani, and Sanja Fidler. Gated-scnn: Gated shape cnns for semantic segmentation. In *ICCV*, pages 5229–5238, 2019. 2
- [37] Kaite Xiang, Kailun Yang, and Kaiwei Wang. Polarization-driven semantic segmentation via efficient attention-bridged fusion. *Optics Express*, 29(4):4802–4820, 2021. 1, 2, 4, 5, 6, 7, 8
- [38] Enze Xie, Wenjia Wang, Wenhai Wang, Peize Sun, Hang Xu, Ding Liang, and Ping Luo. Segmenting transparent object in the wild with transformer. *arXiv preprint arXiv:2101.08461*, 2021. 2
- [39] Enze Xie, Wenhai Wang, Zhiding Yu, Anima Anandkumar, Jose M Alvarez, and Ping Luo. Segformer: Simple and efficient design for semantic segmentation with transformers. *NeurIPS*, 34:12077–12090, 2021. 2, 3, 4, 5, 6, 7
- [40] Ran Yan, Kailun Yang, and Kaiwei Wang. Nlfnet: non-local fusion towards generalized multimodal semantic segmentation across rgb-depth, polarization, and thermal images. In *IEEE ROBOTICS*, pages 1129–1135, 2021. 1, 2, 6, 7
- [41] Changqian Yu, Jingbo Wang, Changxin Gao, Gang Yu, Chunhua Shen, and Nong Sang. Context prior for scene segmentation. In *CVPR*, pages 12416–12425, 2020. 2
- [42] Yuhui Yuan, Lang Huang, Jianyuan Guo, Chao Zhang, Xilin Chen, and Jingdong Wang. Ocnet: Object context for semantic segmentation. *IJCV*, 129(8):2375–2398, 2021. 2
- [43] Hang Zhang, Kristin Dana, Jianping Shi, Zhongyue Zhang, Xiaogang Wang, Amrith Tyagi, and Amit Agrawal. Context encoding for semantic segmentation. In *CVPR*, pages 7151–7160, 2018. 2
- [44] Jiaming Zhang, Kailun Yang, and Rainer Stiefelhagen. Is-safe: Improving semantic segmentation in accidents by fusing event-based data. In *IEEE IROS*, pages 1132–1139, 2021. 2
- [45] Jiaming Zhang, Huayao Liu, Kailun Yang, Xinxin Hu, Ruiping Liu, and Rainer Stiefelhagen. Cmx: Cross-modal fusion for rgb-x semantic segmentation with transformers. *IEEE TITS*, 2023. 1, 2, 3, 5, 6, 7, 8
- [46] Jiaming Zhang, Ruiping Liu, Hao Shi, Kailun Yang, Simon Reiß, Kunyu Peng, Haodong Fu, Kaiwei Wang, and Rainer Stiefelhagen. Delivering arbitrary-modal semantic segmentation. In *CVPR*, pages 1136–1147, 2023. 1, 2, 6, 7, 8
- [47] Qiang Zhang, Shenlu Zhao, Yongjiang Luo, Dingwen Zhang, Nianchang Huang, and Jungong Han. Abmdnet: Adaptive-weighted bi-directional modality difference reduction network for rgb-t semantic segmentation. In *CVPR*, pages 2633–2642, 2021. 1, 2
- [48] Yiyuan Zhang, Kaixiong Gong, Kaipeng Zhang, Hongsheng Li, Yu Qiao, Wanli Ouyang, and Xiangyu Yue. Meta-transformer: A unified framework for multimodal learning. *arXiv preprint arXiv:2307.10802*, 2023. 2, 5
- [49] Hengshuang Zhao, Jianping Shi, Xiaojuan Qi, Xiaogang Wang, and Jiaya Jia. Pyramid scene parsing network. In *CVPR*, pages 2881–2890, 2017. 2
- [50] Sixiao Zheng, Jiachen Lu, Hengshuang Zhao, Xiatian Zhu, Zekun Luo, Yabiao Wang, Yanwei Fu, Jianfeng Feng, Tao Xiang, Philip HS Torr, et al. Rethinking semantic segmentation from a sequence-to-sequence perspective with transformers. In *CVPR*, pages 6881–6890, 2021. 2
- [51] Hao Zhou, Lu Qi, Zhaoliang Wan, Hai Huang, and Xu Yang. Rgb-d co-attention network for semantic segmentation. In *ACCV*, 2020. 2
- [52] Hao Zhou, Lu Qi, Hai Huang, Xu Yang, Zhaoliang Wan, and Xianglong Wen. Canet: Co-attention network for rgb-d semantic segmentation. *PR*, 124:108468, 2022. 1, 2
- [53] Jingkai Zhou, Varun Jampani, Zhixiong Pi, Qiong Liu, and Ming-Hsuan Yang. Decoupled dynamic filter networks. In *CVPR*, pages 6647–6656, 2021. 6, 7
- [54] Wei Zhou, Julie Stephany Berrio, Stewart Worrall, and Eduardo Nebot. Automated evaluation of semantic segmentation robustness for autonomous driving. *IEEE TITS*, 21(5):1951–1963, 2019. 1
- [55] Zhuangwei Zhuang, Rong Li, Kui Jia, Qicheng Wang, Yuanqing Li, and Mingkui Tan. Perception-aware multi-sensor fusion for 3d lidar semantic segmentation. In *ICCV*, pages 16280–16290, 2021. 2